ChemComm
Chemical Communications

Accepted Manuscript

This article can be cited before page numbers have been issued, to do this please use: K. Xia, K. Yatsuzuka, K. Obata, K. Suzuki, K. Takanabe and K. Yamaguchi, *Chem. Commun.*, 2026, DOI: 10.1039/D6CC02380K.

ROYAL SOCIETY OF CHEMISTRY

rsc.li/chemcomm

ChemComm

View Article Online
DOI: 10.1039/D6CC02380K

COMMUNICATION

Polyoxometalate-modified platinum enables enhanced hydrogen evolution in buffered electrolytes

Received 00th January 20xx,
Accepted 00th January 20xx

DOI: 10.1039/x0xx00000x

Kang Xia,*[a§] Koichi Yatsuzuka,[b§¶] Keisuke Obata,[b] Kosuke Suzuki,[a‡] Kazuhiro Takanabe*[b] and Kazuya Yamaguchi *[a]

Hydrogen evolution reaction (HER) under non-extreme pH conditions is attractive but remains kinetically challenging, even for benchmark platinum (Pt) catalysts. Herein, we report that modification with a SiW9 polyoxometalate significantly enhances the HER activity of Pt in near neutral media, as demonstrated in a phosphate-borate buffer (pH 9.2). This enhancement originates from a synergistic co-tuning of the electronic structure and particle size of Pt. This work highlights polyoxometalate modification as an effective strategy for tailoring catalyst properties, enabling efficient HER beyond conventional extreme pH environments.

Water electrolysis is a promising technology for green energy storage and represents a viable route for H_2 production. Current mainstream systems are polymer electrolyte membrane water electrolyzers (PEMWEs)[1–4] and alkaline water electrolyzers (AWEs),[5,6] where the electrolysis is performed under acidic and alkaline conditions, respectively, enabled by advances in catalyst design and the high proton/hydroxide conductivities of the electrolytes. Yet, material corrosion under such extreme pH conditions remains a critical issue, as earth-abundant metal materials are prone to degradation in acidic and/or alkaline environments. This limitation restricts the choice of applicable elements, thereby increasing the cost of the electrolyzers.[7]

An electrolyzer that promotes water splitting under non-extreme pH conditions, where earth-abundant elements such as Fe can be utilized, is highly desirable for reducing the capital costs. Our electrolyte engineering approach focuses on designing the local reaction environment to sustain efficient proton-coupled electron transfer beyond conventional extreme pH conditions.[8] By tailoring buffer identity, concentration, and transport properties, we maximize the diffusional supply of proton donors and acceptors to the electrode interface. This enhances local proton activity, mitigates transport limitations at high current densities, and establishes the electrolyte as an active component that governs reaction kinetics through controlled proton and buffer ion flux.

Compared to the extensive development of catalysts operating under acidic or alkaline conditions, the optimization of the catalyst materials for water electrolysis under near neutral-pH conditions remains underexplored. Owing to the lack of established design principles for catalysts in non-extreme pH environments, largely due to the limited number of studies to date, we considered the modification and tuning of well-established catalysts developed for acidic or alkaline conditions as a primary strategy. Among these, platinum (Pt) nanoparticles are benchmark catalysts for water electrolysis, owing to nearly ideal hydrogen binding energy.[9]

Polyoxometalate (POM), a class of anionic metal oxide clusters with well-defined structures and tunable properties, have been widely used over the past decades to modify the properties of various metal nanoparticle catalysts.[10–14] We demonstrated that robust electronic interactions between surface-anchored multidentate POM $[SiW_9O_{34}]^{10-}$ (**SiW9**) and metal nanoparticles, such as gold[15,16], palladium,[17] and gold–silver alloy,[18] enhance their catalytic activity and stability. This enhancement arises from the high negative charge and multiple coordination sites of **SiW9** (Fig. 1a). Following this sol-gel strategy, Wei *et al.* validated the HER performance of **SiW9**-protected-Pt nanoparticle catalyst in PEMWEs.[19] However, this sol-gel synthesis requires careful control of reaction parameters such as concentration, temperature, and loading amount (Fig. 1a), which limits its extensions to practical applications.

Here, we report the enhanced HER activity of Pt modified with **SiW9** in a near neutral buffer (pH 9.2). Commercial Pt nanoparticles (Pt/Vulcan) were simply immersed in an aqueous solution of **SiW9** to afford the modified catalyst, denoted as **SiW9**-Pt/Vulcan (Fig. 1b). Comparison of the adsorption behavior of **SiW9** with that of plenary POMs, based on STEM-EDS mapping and elemental analysis, suggests that the coordinative structure of **SiW9** provides an essential anchoring function onto Pt nanoparticles. The pronounced HER

[a] *Department of Applied Chemistry, School of Engineering, The University of Tokyo, 7-3-1 Hongo, Bunkyo-ku, Tokyo 113-8656, Japan.*
[b] *Department of Chemical System Engineering, School of Engineering, The University of Tokyo, 7-3-1 Hongo, Bunkyo-ku, Tokyo 113-8656, Japan.*
§Co-first author
¶Current affiliation: National Institute for Materials Science, Research Center for Energy and Environmental Materials, 1-1 Namiki, Tsukuba, Ibaraki, 305-0044, Japan
‡Current affiliation: Department of Advanced Materials Science, Graduate School of Frontier Sciences, The University of Tokyo, 5-1-5 Kashiwanoha, Kashiwa, Chiba 277-8561, Japan.
† *Electronic Supplementary Information (ESI) available.*
See DOI: 10.1039/x0xx00000x

performance of **SiW9**-Pt/Vulcan was confirmed by diffusion-controlled electrolysis using a rotating disk electrode (RDE) and device-oriented electrolysis using carbon paper. This method was applied to another benchmark catalyst, Ru/Vulcan, for enhanced HER performance, demonstrating the applicability of this approach. Electrochemical analysis, IR, TEM, STEM-EDS, and XPS reveal that the significant improvement in HER activity of Pt—already near the apex of the HER volcano plot[20]—is likely attributed to a co-tuning effect of electronic states and particle size induced by **SiW9** adsorption. This facile strategy not only elucidates the intrinsic effect of multidentate POMs but also provides an effective approach for optimizing a wide range of HER catalysts via POM adsorption, even when they are already close to the apex of the catalytic volcano plots.

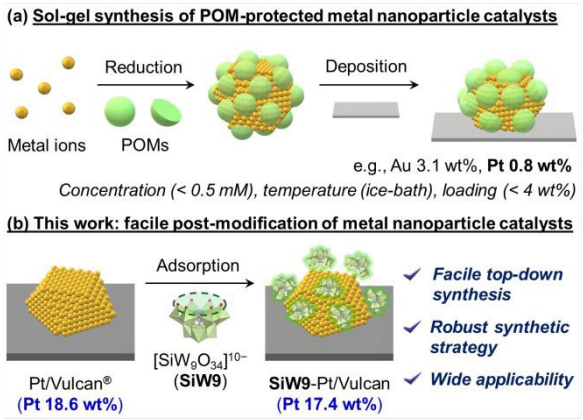

Fig. 1 (a) Conventional sol-gel synthesis of POM-protected metal nanoparticle catalysts. (b) This work: automatic modification of metal nanoparticle catalysts with multidentate POMs by a facile post-modification method.

SiW9 was selectively adsorbed onto Pt nanoparticles by a simple immersion method. Specifically, Pt/Vulcan was immersed in an aqueous solution of the sodium salt of **SiW9** ($Na_{10}SiW_9O_{34}$) at room temperature, followed by filtration and washing with excessive water to obtain **SiW9**-Pt/Vulcan (Fig. 1b). The **SiW9** retrieved from the filtrate was subjected to IR analysis, and characteristic bands derived from **SiW9** exhibited no significant peak shift, demonstrating that its structural integrity was maintained during the catalyst modification process (Fig. S1). TEM images revealed that **SiW9**-Pt/Vulcan retained a particle size of 2.3 ± 0.4 nm (Fig. 2a,b,S2) without noticeable agglomeration, thereby minimizing the influence of particle size on subsequent HER performance evaluations. Then, STEM-EDS mapping images showed a homogeneous distribution of Pt and W in **SiW9**-Pt/Vulcan (Fig. 2c), confirming the successful adsorption of **SiW9** onto Pt nanoparticles.

According to ICP-AES analysis, the loading amount of the Pt catalysts were confirmed: Pt/Vulcan contained 18.6 wt% Pt, while **SiW9**-Pt/Vulcan contained 17.4 wt% Pt and 4.5 wt% W, indicating that no loss of Pt occurred during the POM modification (Table S1). Notably, the molar ratio of **SiW9** to Pt was determined to be 3.1:100, corresponding to an estimated surface coverage of approximately 50% (Fig. S3; see ESI for details), which is consistent with our previous reports on **SiW9**-modified Au nanoparticles.[15,16] On the contrary, when plenary POMs such as $[SiW_{12}O_{40}]^{4-}$ (**SiW12**) or $[Nb_6O_{19}]^{8-}$ (**Nb6**) were utilized in place of **SiW9** in this simple immersion method, almost no adsorption of these POMs was observed, as evidenced by ICP-AES analysis and STEM-EDS mapping (Fig. S4, Table S2). Considering the structural similarity of **SiW12** and the comparable charge density of **Nb6** to those of **SiW9**, this difference is attributed to the specific interaction between metal nanoparticles and multidentate POMs, as established in previous studies by our group and others.[15–19] Furthermore, **SiW9**-Pt/Vulcan was immersed in the electrolyte solution (pH 9.2, 0.5 mol kg^{-1} K-phosphate + 1.5 mol kg^{-1} K-borate),[21] and ICP-AES analysis confirmed that negligible amounts of Pt and W leached into the solution, indicating the high stability of the modified catalyst under operating conditions (Table S3).

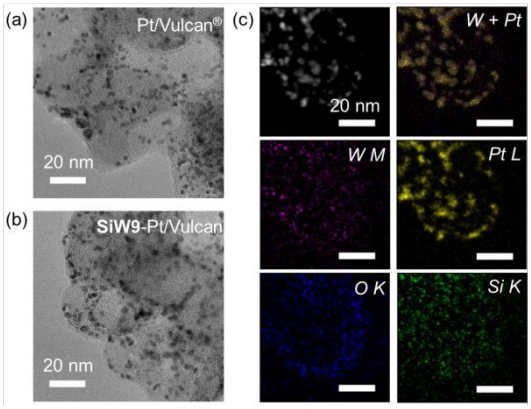

Fig. 2 TEM images of (a) Pt/Vulcan and (b) **SiW9**-Pt/Vulcan. (c) STEM-EDS mapping images of **SiW9**-Pt/Vulcan.

The HER activity of Pt/Vulcan with and without **SiW9** modification was examined using chronopotentiometry (CP).[21] To rule out the possibility of diffusion limitations and to isolate the effects of changes in electronic nature, a rotating disk electrode (RDE) system was employed, allowing precise control of mass transport. The rotation rate was set to 3600 rpm, at which the rotation speed had no significant effect on the required potential (Fig. 3a), thereby excluding contributions from ion diffusion-related phenomena. The CP results, in the presence and absence of **SiW9**, demonstrate a substantial enhancement in the catalytic activity. The overpotential at 10 mA cm^{-2} decreased from 130 to 81 mV (Fig. 3b), indicating that this post-modification with **SiW9** significantly improves the HER performance of Pt nanoparticle catalysts.

The change in Tafel slopes indicates a kinetic modification induced by the presence of **SiW9** on Pt nanoparticles. Although buffered electrolytes do not completely eliminate diffusion-induced overpotentials,[22,23] the apparent Tafel slopes were compared to elucidate the effects of **SiW9**. The apparent Tafel slopes in the linear Tafel region (log $|j|$ = 0.7–1.1) were 107.8 mV dec^{-1} and 160.1 mV dec^{-1} with and without **SiW9** adsorption, respectively (Fig. 3b). The significant decrease in the Tafel slope can be rationalized by either an increase in the coverage of reaction intermediates with increasing overpotential, an intrinsic increase in the charge transfer coefficient of the rate-determining step (RDS), or a switch of the RDS to another elementary step. The surface coverage is governed by the

relative rates of formation and consumption of the corresponding intermediates, while the charge transfer coefficient reflects the potential sensitivity of the reaction barrier. Likewise, a switch in the RDS arises from the changes in the relative rates of competing elementary steps. Therefore, although the precise origin of the Tafel slope change cannot be uniquely identified in the present study, all of these possibilities are closely related to kinetic phenomena governed by the electronic properties of the catalyst.

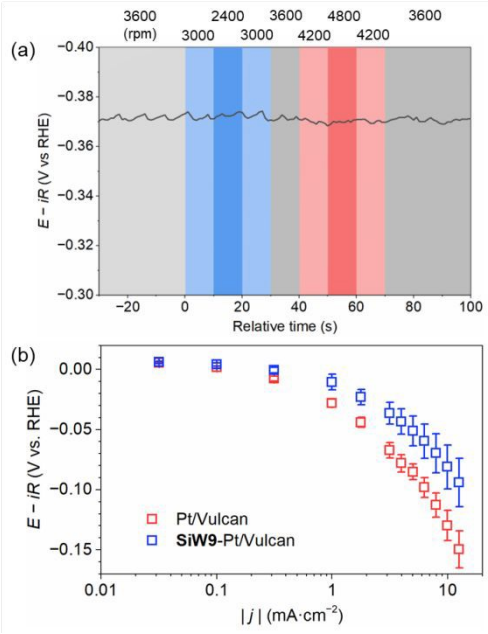

Fig. 3 (a) Independence of the HER rate on rotation speed for Pt/Vulcan at 100 mA cm^{-2} in an aqueous buffer solution at pH 9.2 of 0.5 mol kg^{-1} K-phosphate + 1.5 mol kg^{-1} K-borate at 80 °C with H_2 bubbling. Note: in order to obtain a stable state of the potential applied and exclude the effect of possible catalyst degradation, the RDE GC electrode was performed at 100 mA cm^{-2} for 30 min before changing the rotation rate. As no obvious effect of rotation speed was observed in 100 mA cm^{-2}, a much higher current than those in the Tafel plot region, it is clear that no effect of rotation speed for Pt/Vulcan exists at 10 mA cm^{-2}. Since Pt/Vulcan possessed lower activity than **SiW9**-Pt/Vulcan, it is evident that there is also no effect of rotation speed at 10 mA cm^{-2} for **SiW9**-Pt/Vulcan. (b) Tafel plots of the Pt/Vulcan/GC RDE electrode (blue) and the **SiW9**-Pt/Vulcan/GC electrode (red) in an aqueous buffer solution at pH 9.2 of 0.5 mol kg^{-1} K-phosphate + 1.5 mol kg^{-1} K-borate at 70 °C with H_2 bubbling, based on chronopotentiometry measurements. The loading amount of Pt on RDE is 2.5 μg cm^{-2}.

Having demonstrated that **SiW9** enhances the HER activity of Pt nanoparticles, we evaluated the availability of this method under industrially relevant conditions (Fig. S5). Despite the involvement of the diffusion effect—particularly given the high activity of **SiW9**-Pt/Vulcan—the adsorption of **SiW9** onto the Pt nanoparticle catalyst still led to a significant improvement in catalytic performance. Specifically, the overpotential decreased from −0.64 to −0.55 V *vs* RHE at a current density of 1 A cm^{-2} (Fig. S5), which is qualitatively consistent with the behaviors observed in the RDE system. The relatively large Tafel slope values in the high-current-density region (100–1000 mA cm^{-2}; > 400 mV dec^{-1} with or without **SiW9**) suggest that mass-transport-related phenomena are involved, likely associated with local pH shifts at the electrode surface and corresponding shifts in the equilibrium potential of the HER.[24] The effects of POM may include mitigating local pH changes even at high current densities, effectively mimicking the function of an ionomer by acting as a surface-confined buffer anion species.

The durability of **SiW9**-Pt/Vulcan under water electrolysis conditions relevant to practical applications was further evaluated by chronopotentiometry (Fig. 4). The results confirm a clear and sustained improvement in the catalytic performance of Pt for at least 5 h. Particularly, the potential loss at 400 mA cm^{-2} was nearly negligible for **SiW9**-Pt/Vulcan, whereas a loss of approximately 15% was observed for Pt/Vulcan (Fig. S6). In addition, **SiW9**-Pt/Vulcan showed improved resistance toward repeated ON/OFF operation compared with Pt/Vulcan (Fig. S7). These results indicate that the adsorption of POMs onto Pt nanoparticles is sufficiently robust over this timescale, even under the industrial level-current density conditions.

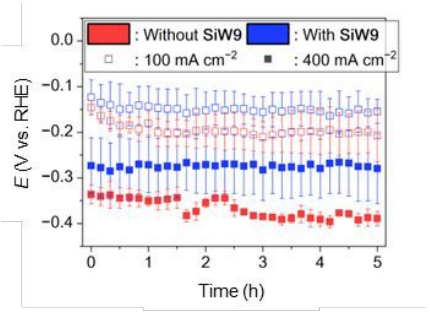

Fig. 4 The durability test of the time-dependent potential curve of Pt/Vulcan/carbon paper (red) and the **SiW9**-Pt/Vulcan/carbon paper (blue) in an aqueous buffer solution at pH 9.2 containing 0.5 mol kg^{-1} K-phosphate + 1.5 mol kg^{-1} K-borate at 80 °C with H_2 bubbling, based on chronopotentiometry measurements. The loading amount of Pt on the carbon paper is 0.3 mg cm^{-2}. The Pt ratio in the loaded Pt/Vulcan is 40% (w/w).

The sizes of Pt nanoparticles after 5 h of electrolysis at 400 mA cm^{-2} were evaluated by TEM. No significant change in particle size was observed for **SiW9**-Pt/Vulcan (2.4 ± 0.4 nm), whereas pronounced agglomeration of Pt nanoparticles was observed for Pt/Vulcan (4.4 ± 1.1 nm, Fig. 2a,b,S8). Furthermore, STEM-EDS mapping images revealed that **SiW9**-Pt/Vulcan remained its core-shell-like structure and that no obvious aggregation of **SiW9** into WO_x nanoparticles occurred after electrolysis (Fig. S9). Meanwhile, the recovered species in **SiW9**-Pt/Vulcan after the reaction using a salting-out method,[19] maintained the characteristic bands derived from **SiW9** (Fig. S10), demonstrating that the structural integrity of **SiW9** was maintained during the reaction. These results indicate that the adsorption of **SiW9** not only enhances the catalytic activity of Pt but also improves its stability during electrolysis. Although Pt/Vulcan has been widely employed as a cathode catalyst, the observed agglomeration of Pt nanoparticles in the near neutral buffer media (0.5 mol kg^{-1} K-phosphate + 1.5 mol kg^{-1} K-borate) highlights the necessity of POM-based modification under near neutral pH conditions.

In addition, this facile adsorption method was extended to another commercial catalyst, Ru/Vulcan. TEM images revealed that the Ru nanoparticles retained their particle size at approximately 2.7 nm (Fig. S11), while enhanced HER activity was observed using an RDE system (Fig. S12). An increase in activity was also observed when a Ru/Vulcan-deposited glassy

carbon electrode was immersed in a solution of **SiW9** (Fig. S13), supporting the effectiveness of this POM modification strategy.

XPS is widely used to investigate the electronic structures of metal nanoparticles, and shifts to higher binding energy (BE) are commonly interpreted as indicative of decreased electron density[16,19,25,26]. The peaks observed at around 72 eV and 75 eV in the Pt 4*f* region, corresponding to $4f_{5/2}$ and $4f_{7/2}$, respectively, can be attributed to a mixed oxidation state of Pt^0 and $Pt^{\delta+}$ (Fig. 5),[26] suggesting partial oxidation of Pt upon exposure to air. Compared to Pt/Vulcan (BE = 71.4 eV for Pt^0 and 72.6 eV for $Pt^{\delta+}$), **SiW9**-Pt/Vulcan exhibited higher BE values (71.6 eV for Pt^0 and 72.7 eV for $Pt^{\delta+}$), indicating a decrease in the electronic density of Pt after **SiW9** modification. Consistently, the $Pt^{\delta+}/Pt^0$ ratio (0.89) was significantly higher than that for Pt/Vulcan (0.58), supporting this conclusion. Since no significant change in particle size was observed upon **SiW9** adsorption (Fig. 2), the BE shift is attributed to electron transfer from Pt nanoparticles to the **SiW9** ligands, consistent with observations in sol–gel-derived systems.[19] A similar modulation of electronic states was observed for Ru/Vulcan after **SiW9** modification, as evidenced by XPS, further supporting this interpretation (Fig. S11).

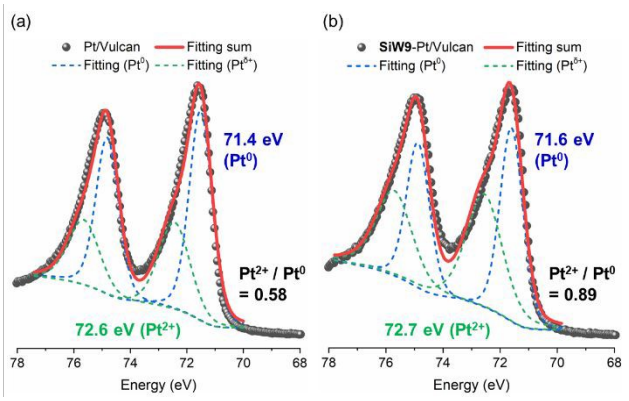

Fig. 5 XPS spectra of Pt *4f* orbital for (a) Pt/Vulcan and (b) **SiW9**-Pt/Vulcan.

Finally, we discuss the enhancement effect of **SiW9** on the HER performance of Pt nanoparticles in terms of three key factors. The first is the suppression of particle agglomeration. TEM images after electrolysis reveal that **SiW9** serves as a dual role in stabilizing Pt nanoparticles while maintaining their high catalytic activity. The second factor is the electron-withdrawing nature of **SiW9**, as reflected in changes in kinetic parameters observed in electrochemical measurements. XPS analysis indicates a decrease in the electron density of Pt nanoparticles after **SiW9** adsorption, which may optimize the Pt–H binding strength and thereby intrinsically enhance HER activity. The third factor is the unique multielectron transfer capability of POMs, which may further promote H_2 production by facilitating mass transport.[27–29] Overall, given that Pt is widely recognized to lie near the apex of the HER volcano plot—where hydrogen adsorption on Pt is slightly exothermic—the present POM-modification strategy, which fine-tunes the Pt–H binding interaction, represents a crucial yet challenging step toward further approaching the ideal apex of HER catalysts.

We gratefully acknowledge the financial support from GteX Program Japan (Grant Number JPMJGX23H2), JSPS KAKENHI (24KJ0563 and 22H04971), and Mizuho Foundation for the Promotion of Sciences. A part of this work was supported by Advanced Research Infrastructure for Materials and Nanotechnology in Japan (ARIM) of the Ministry of Education, Culture, Sports, Science and Technology (MEXT), JPMXP1224UT0038 and JPMXP1225UT0084. We thank Ms. Mari Morita and Mr. Hiroyuki Oshikawa (The University of Tokyo) for their assistance with the STEM-EDS analysis. We also thank Ms. Vo Tran Thanh Ngoc (Vietnam National University), Ms. Atmadja Kimberly (Nanyang Technological University), and Mr. Kumar Srikant (Indian Institute of Technology Roorkee) for their experimental support on electrochemical measurements.

Conflicts of interest

There are no conflicts to declare.

Data availability

The data supporting this article has been included as part of the SI.

References

1 R. J. Ouimet, J. R. Glenn, D. De Porcellinis, A. R. Motz, M. Carmo and K. E. Ayers, *ACS Catal.*, 2022, **12**, 6159–6171.
2 K. Ayers, N. Danilovic, R. Ouimet, M. Carmo, B. Pivovar and M. Bornstein, *Annu. Rev. Chem. Biomol. Eng.*, 2019, **10**, 219–239.
3 J. Kibsgaard and I. Chorkendorff, *Nat. Energy*, 2019, **4**, 430–433.
4 A. Li, S. Kong, K. Adachi, H. Ooka, K. Fushimi, Q. Jiang, H. Ofuchi, S. Hamamoto, M. Oura, K. Higashi, T. Kaneko, T. Uruga, N. Kawanuma, D. Hashizume and R. Nakamura, *Science*, 2024, **384**, 666–670.
5 M. David, C. Ocampo-Martínez and R. Sánchez-Peña, *J. Energy Storage*, 2019, **23**, 392–403.
6 F. Liu, K. Miyatake, M. Tanabe, A. M. A. Mahmoud, V. Yadav, L. Guo, C. Y. Wong, F. Xian, T. Iwataki, M. Uchida and K. Kakinuma, *Adv. Sci.*, 2024, **11**, 2402969.
7 L. Bertuccioli, A. Chan, D. Hart, F. Lehner, B. Madden and E. Standen, *Development of Water Electrolysis in the European Union*, 2014.
8 T. Shinagawa, M. T.-K. Ng and K. Takanabe, *ChemSusChem*, 2017, **10**, 4155–4162.
9 J. K. Nørskov, T. Bligaard, A. Logadottir, J. R. Kitchin, J. G. Chen, S. Pandelov and U. Stimming, *J. Electrochem. Soc.*, 2005, **152**, J23.
10 A. S. Cherevan, S. P. Nandan, I. Roger, R. Liu, C. Streb, D. Eder, *Adv. Sci.*, 2020, **7**, 1903511.
11 K. Xia, K. Yamaguchi and K. Suzuki, *Angew. Chem. Int. Ed.*, 2023, **62**, e202214506.
12 C. Martin, K. Kastner, J. M. Cameron, E. Hampson, J. Alves Fernandes, E. K. Gibson, D. A. Walsh, V. Sans and G. N. Newton, *Angew. Chem. In. Ed.*, 2020, **59**, 14331–14335.
13 Y. Wang, A. Neyman, E. Arkhangelsky, V. Gitis, L. Meshi and I. A. Weinstock, *J. Am. Chem. Soc.*, 2009, **131**, 17412–17422.
14 Y. Lin and R. G. Finke, *J. Am. Chem. Soc.*, 1994, **116**, 8335–8353.
15 K. Xia, T. Yatabe, K. Yonesato, S. Kikkawa, S. Yamazoe, A. Nakata, R. Ishikawa, N. Shibata, Y. Ikuhara, K. Yamaguchi and K. Suzuki, *Nat. Commun.*, 2024, **15**, 851.

View Article Online
DOI: 10.1039/D6CC02380K

16 K. Xia, T. Yatabe, K. Yonesato, T. Yabe, S. Kikkawa, S. Yamazoe, A. Nakata, K. Yamaguchi and K. Suzuki, *Angew. Chem. Int. Ed.*, 2022, **61**, e202205873.
17 K. Xia, T. Yatabe, K. Yamaguchi and K. Suzuki, *Dalton Trans.*, 2024, **53**, 11088–11093.
18 K. Xia, T. Yatabe, K. Yonesato, K. Kawakami, S. Kikkawa, S. Yamazoe, K. Yamaguchi and K. Suzuki, *Small*, 2026, **22**, e14728.
19 H. Shen, Y. Huang, P. Zhao, R. Gao, Z. Wei, X. Gao, M. Liao, W. Dai, X. Liu, D. Sui, J. Liu, S. Zhu and Y. Wei, *Adv. Funct. Mater.*, 2026, **36**, e14862.
20 S. Trasatti, *J. Electroanal. Chem. Interfacial Electrochem.*, 1972, **39**, 163–184.
21 Note: in the present study, borate was selected as the main buffer component because (i) its pKa is suitable for near-neutral HER operation, (ii) concentrated borate solutions exhibit lower viscosity than phosphate-based electrolytes, thereby suppressing solution resistance, and (iii) borate is volatile and therefore advantageous from a practical viewpoint. Meanwhile, phosphate was introduced as a secondary buffer component because phosphate species are known to contribute to the formation of protective passive layers on anode materials. Although phosphate does not significantly affect the HER activity in the present cathodic system, it was used with future practical electrolysis applications in mind. The operating pH of 9.2 was selected based on the pKa of the borate buffer system.
22 T. Shinagawa, K. Obata and K. Takanabe, *ChemCatChem*, 2019, **11**, 5961–5968.
23 K. Obata, L. Stegenburga and K. Takanabe, *J. Phys. Chem. C*, 2019, **123**, 21554–21563.
24 M. Wada, K. Obata and K. Takanabe, *EES Catal.*, DOI: 10.1039/D6EY00006A.
25 H. Wang, L. Wang, D. Lin, X. Feng, Y. Niu, B. Zhang and F.-S. Xiao, *Nat. Catal.*, 2021, **4**, 418–424.
26 E. I. Vovk, A. V. Kalinkin, M. Yu. Smirnov, I. O. Klembovskii and V. I. Bukhtiyarov, *J. Phys. Chem. C*, 2017, **121**, 17297–17304.
27 L. Yang, S. Zhang, K. Li, H. Wu, T. Wu, D. Wu and J. Chen, *Energy Storage Mater.*, 2024, **65**, 103149.
28 B. Rausch, M. D. Symes, G. Chisholm and L. Cronin, *Science*, 2014, **345**, 1326–1330.
29 M. Raula, S. Dabush Avnaim, A. Kar, M. Samin, S. Roy, M. Baranov, N. Leffler, Z.-L. Lang, J. M. Poblet and I. A. Weinstock, *J. Am. Chem. Soc.*, 2025, **147**, 24653–24661.

View Article Online
DOI: 10.1039/D6CC02380K

The data supporting this article have been included as part of the Supplementary Information